Original Paper

Landslides (2025) 22:619–635
DOI 10.1007/s10346-024-02328-3
Received: 5 February 2024
Accepted: 18 July 2024
Published online: 16 August 2024
© The Author(s) 2024

Yuting Liu · Lorenzo Brezzi · Zhipeng Liang · Fabio Gabrieli · Zihan Zhou · Simonetta Cola

Image analysis and LSTM methods for forecasting surficial displacements of a landslide triggered by snowfall and rainfall

Abstract Landslide-prone areas, predominantly located in mountainous regions with abundant rainfall, present unique challenges when subject to significant snowfall at high altitudes. Understanding the role of snow accumulation and melting, alongside rainfall and other environmental variables like temperature and humidity, is crucial for assessing landslide stability. To pursue this aim, the present study focuses first on the quantification of snow accumulated on a slope through a simple parameter obtained with image processing. Then, this parameter is included in a slope displacement prediction analysis carried out with long short-term memory (LSTM) neural network. By employing image processing algorithms and filtering out noise from white-shown rocks, the methodology evaluates the percentage of snow cover in RGB images. Subsequent LSTM forecasts of landslide displacement utilize 28-day historical data on rainfall, snow, and slope movements. The presented procedure is applied to the case of a deep-seated landslide in Italy, a site that in winter 2020–2021 experienced heavy snowfall, leading to significant snow accumulation on the slope. These episodes motivated a study aimed at forecasting the superficial displacements of this landslide, considering the presence of snow both at that time and in the following days, along with humidity and temperature. This approach indirectly incorporates snow accumulation and potential melting phenomena into the model. Although the subsequent winters were characterized by reduced snowfall, including this information in the LSTM model for the period characterized by snow on the slope demonstrated a dependency of the predictions on this parameter, thus suggesting that snow is indeed a significant factor in accelerating landslide movements. In this context, detecting snow and incorporating it into the predictive model emerges as a significant aspect for considering the effects of winter snowfall. The method aims to propose an innovative strategy that can be applied in the future to the study of the landslide analyzed in this paper during upcoming winters characterized by significant snowfall, as well as to other case studies of landslides at high altitudes that lack precise snow precipitation recording instruments.

Keywords Displacement forecasting · Snowmelt · LSTM · Landslide triggering · Images recognition · Smart monitoring

Introduction

Landslide disasters are widely distributed throughout the world (Kirschbaum et al. 2009). Some landslides occur within reservoirs and are influenced by long-term fluctuations in water level (Zou et al. 2023; Ye et al. 2024a). Some are reactivated and triggered due to earthquakes and deformed by rainfall (Sassa et al. 2005; Yin et al. 2009). In the Alps region of Europe, snow, temperatures, and humidity pose challenges to the stability of landslides during transitional seasons characterized by a warming climate (Guzzetti 2000). Although rainfall is generally the main natural agent triggering landslides, in high-altitude countries and regions, snowfall and snowmelt are essential factors in considering the study of geological hazards (Has et al. 2012; Bajni et al. 2021). Therefore, identifying the individual contributions of various hydrometeorological factors to accelerated movements is key to landslide research (Jakob et al. 2006; Ye et al. 2024b). In particular, landslides in frozen areas have been closely related to various meteorological and hydrological phenomena; winter blizzards, soil freeze-thaw cycles, and snowmelt water infiltration play pivotal roles (Subramanian et al. 2017; Hinds et al. 2021). Snowfall and accumulation on a slope can generate an additional load on the ground and induce instability. However, since temperatures are generally below zero, the additional resistance due to the soil freezing can partially compensate for the increased load (Harris et al. 2009). In addition, the thaw that occurs when temperatures rise in spring or on warmer days can generate water infiltration that cannot be easily accounted for in the hydrological balance of a slope.

Previous studies have reported evidence that anomalous spring and landslide events induced by snowmelt are clearly linked to warming (Durand et al. 2009; Saez et al. 2013; Xian et al. 2022). The important role of the dynamics controlling the atmosphere-surface interactions, which affected snowmelt processes and soil freezing-thawing cycles, is evidenced by Subramanian et al. (2020) and Xian et al. (2022). Also, Matsuura et al. (2003) considered meteorological factors, particularly snowmelt, in their landslide research and confirmed that snowmelt influences landslide displacement. The hydrological behavior of landslides, considering both snowpack and meteorological factors, has also been studied by Osawa et al. (2017) and Okamoto et al. (2018). They found that the pore water pressure response to the snow loading is strongly affected by the sliding mass permeability, which in turn is influenced by seasonal changes. Furthermore, Osawa et al. (2024) proposed a simplified semi-empirical hydrological model for landslide pressure response, aiming to predict the short-term response of pore pressure to rainfall and/or snowmelt inputs.

A comprehensive consideration of interrelated factors affecting the thermal-hydraulic-mechanical behavior of a landslide is indispensable for understanding and predicting landslide occurrences in frozen terrains. However, quantifying snowfall or snowmelt is challenging due to monitoring methods and the stochastic nature of the environment. Martelloni et al. (2012) have proposed an integration

of a simple snow accumulation-melting model (SAMM) with landslide warning systems that utilize empirical rainfall thresholds. This model overcomes the gap between physically based models and the empirical temperature index models based on the traditional pluviometer monitoring combined with temperature data. Accordingly, snow accumulation is considered and integrated into a regional-scale early warning system that relies on statistical rainfall thresholds to predict landslide occurrences in the Emilia Romagna region (Italy) with the SAMM model. Another study has been carried out on a mountain basin nearby Champoluc in the Val D'Aosta region in Italy (Panzeri et al. 2022). The objective of evaluating the influence of snowmelt and precipitation on the development of shallow landslides was achieved by statistically comparing in situ meteorological observations with laboratory analyses. Cutting-edge weather and snowpack stations were utilized to conduct comprehensive analyses of snowmelt and meteorological data. The snowmelt plus atmospheric conditions such as temperature and humidity were integrated to intuitively observe the interaction between snow and soil. Chiarelli et al. (2023), instead, examined the case of the Tartano basin in Lombardia (Italy). There, the landslide susceptibility prediction accuracy improved by 5% when involving snowmelt factor obtained with a traditional mechanical model that mimics the triggering mechanism of shallow landslides. Although the research studies demonstrated the significant influence of snow on landslide kinematics and some of them suggested and implemented monitoring methods and quantitative measures to consider the snow effects, they were unable to assess a standard methodology for considering the snow's influence on the dynamics of a landslide or on a forecasting tool.

Moreover, even if many scholars indicated that the snowmelt affected the landslide stability more than snow accumulation, snowmelt remains difficult to be allowed for landslide assessment because it cannot be directly measured by using traditional equipment, such as the heated rain gauge. Moving from the basic idea that the snow melting is related to the variation of snow accumulated on the slope surface, the authors suggest a procedure based on image processing for evaluating the actual amount of snow present on landslides and we try to apply this method on the case study of Sant'Andrea landslide, a deep-seated landslide in the North-East of Italy. This slope is chosen because, in addition to traditional monitoring tools, there is a terrestrial digital photographic system collecting RGB images of the slope for 3 years with the aim of using them as a monitoring dataset.

The use of photogrammetry within the monitoring procedure for landslide is a strategy that has already proven effective both on the Sant'Andrea landslide and on another Italian landslide (Gabrieli et al. 2016; Brezzi et al. 2020, 2021b). In these previous applications, the images were processed through some image processing and digital correlation algorithms finalized to reconstruct the 2D displacement field on the image plane and subsequently to project it onto the three-dimensionality of the scene. Broadly speaking, the applications of photogrammetry monitoring methods for landslides are increasing (Pan 2018). There are significant breakthroughs in multi-view photogrammetry, leading to the development of a novel category of algorithms and software tools that enable enhanced automation in surface reconstruction, feature detection, and displacement monitoring. These cutting-edge techniques potentially offer topographic information to be used in geoscience applications, all while drastically reducing costs compared to some traditional methods such as topographic and laser scanning surveys (Stumpf et al. 2015). Moreover, the efficacy of integrating digital photogrammetry with geological data to enhance the characterization and comprehension of landslide mechanisms is noticeable. Consequently, this knowledge can contribute to the identification and formulation of effective mitigation strategies (Laribi et al. 2015).

When analyzing large numbers of images, the algorithm must be efficient and swift, based on determining simple yet descriptive quantities. For this reason, to precisely measure the volume change in snow accumulation and melting, a dimensionless indicator called Pixel Volume Index (PVI) is here introduced to accurately represent variations in snow cover. The concept of Pixel Volume (PV) was initially employed to achieve video deblurring and the state-of-the-art performance both quantitatively and qualitatively (Son et al. 2021). Here, PVI is utilized and refined to quantify the snow volume, aiming to clearly depict the actual condition of snow presence on the slope. The model, which integrates photogrammetry monitoring with deep learning using PVI as a link, holds significant potential and development space for predicting landslide displacement.

Next, once the quantification of the snow on the slope has been obtained, it is then used, together with other quantities such as temperature, humidity, and rainfall, as input of a model that forecasts the landslide displacements. Deep learning (DL) is an effective method for forecasting in many domains including geohazards (LeCun et al. 2015; Mondini et al. 2023; Nava et al. 2023; Liu et al. 2024). Even more recently, it has also been introduced in the detection and evaluation of landslide susceptibility (Feizizadeh et al. 2021; Sameen et al. 2020). Within DL, convolutional neural networks (CNNs) are most frequently used and behave the best in the image feature extraction (Bishop 1995). Therefore, they are frequently used for processing remote-sensing image dataset (Prakash et al. 2020; Ngo et al. 2021). However, unlike image data, matching time series data for use by CNNs can be difficult. To solve this, Teza et al. (2022) processed the time series data and transformed them into figures, in the shape of scalograms, with dimensions of $224 \times 224 \times 3$. In this way, they were able to use a CNN to extract features and to obtain successful predictions of the surficial displacements of the Sant'Andrea landslide.

However, to establish a multi-factor landslide prediction model, CNNs can no longer undertake this task due to the resolution limitations of images. Thus, another DL method, the long short-term memory (LSTM) neural network, is introduced and applied to landslides located in the Three Gorges reservoir (Xu and Niu 2018; Yang et al. 2019). As a type of recurrent neural network (RNN) (Medsker and Jain 1999), LSTM can capture long-term dependencies in various time series data (Van Houdt et al. 2020), leveraging contextual information while establishing mappings between input and output sequences (Hochreiter and Schmidhuber 1997). Moreover, the architecture of LSTM can be modified and extended according to the requirements of the task. In practical applications, multiple LSTM layers can be stacked to enhance the model's representational capacity (Graves 2012).

In the study here presented, in consideration of many involved factors such as rainfall, snow (PVI), temperature, and humidity, different combinations and training durations are attempted to test

and improve the accuracy of LSTM predictions of the Sant'Andrea landslide's movement.

Methodology

This methodology integrates several approaches from different fields for photogrammetric computation and machine learning. In the section on landslide monitoring, the primary focus is on the collection and pre-processing of image monitoring and geodetic measurement data. Within the early warning part, image processing techniques, machine learning, and deep learning are effectively combined into a comprehensive system. As depicted in Fig. 1, initial data collection involves several monitored parameters of the landslide, including rainfall, temperature, humidity, and displacement (yellow circle). The directly detected quantities can also include the images acquired by the photographic system aimed at monitoring the slope. In order to quantify the snow and generate usable data related to the snow quantity on the slope, since this cannot be directly monitored, image data from monitoring is compiled and processed to compute a Pixel Volume Index (PVI) for snow quantification (green boxes). All these quantities, image datasets, and elaboration results, directly collected and then processed, are included in the yellow dashed circle. Lastly, all the collected data are used as input into a customized LSTM neural network for the identification of the most suitable approach for predicting future displacements (red boxes).

Pixel volume index

Due to the absence of dedicated snow monitoring devices, in the present work, the quantification of snow cover is determined using the Pixel Volume Index (PVI), a parameter that quantifies the current presence of snow on the slope (see brief explanation below). Figure 2a represents a schematic scene to be processed, whereas Fig. 2b and c represent two important features necessary for snow quantification: an estimation of the snow thickness proportion and a percentage evaluation of the base area occupied by snow, detected on a representative patch of the image. These two quantities, named S_T and S_C respectively, allow the definition of a variable, denoted as snow PVI, obtained by directly multiplying S_T and S_C.

The processes of obtaining snow coverage S_C and snow thickness S_T follow two distinct paths, each made up of several steps. When utilizing image analysis tools as a foundation, the first two specific areas must be masked, named A_C and A_T, as depicted in Fig. 2, respectively, for the evaluation of S_C and S_T.

A first approximation of snow coverage estimation could be obtained by counting the number of white pixels present in the masked area A_C. Nonetheless, when analyzing the image dataset, different levels of exposure or lighting of the photo, the cloudy or sunny condition of the area, and different colors in different seasons make the identification of the level of "white" contained in the pixels ambiguous. The direct consequence of this is an unreliable quantification of snow coverage. Furthermore, if there are other white objects on the scene, such as rocks and walls, these could hinder the code, resulting in a false recognition of the snow and consequent erroneous quantification of the S_C parameter. To overcome these problems, before counting the number of white pixels in the A_C area, a specific algorithm is implemented to categorize the type of image in terms of illumination and overall coloration. For each image category, then, specific thresholds are searched for identifying the RGB contents which indicate the presence of "white" corresponding to snow and "white" corresponding to other objects. The algorithm used both for identifying the type of image and for recognizing the "white" corresponding to snow is based on the analysis of the red and blue contents of the pixels in the cropped area A_C. In particular, it is possible to plot the information contents relating to all the pixels included in A_C in a graph having red/blue in

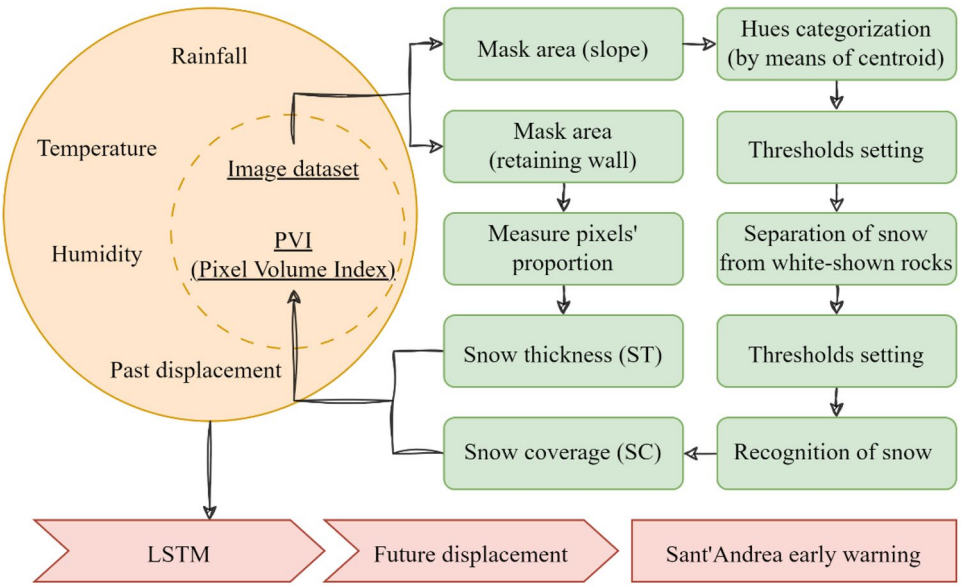


Fig. 1 Early warning system considering snow. The design is composed of three subsystems: monitored quantities are represented in the yellow circle; image recognition algorithms for snow estimation are shown in green; and the deep learning forecasting system is depicted in red shapes

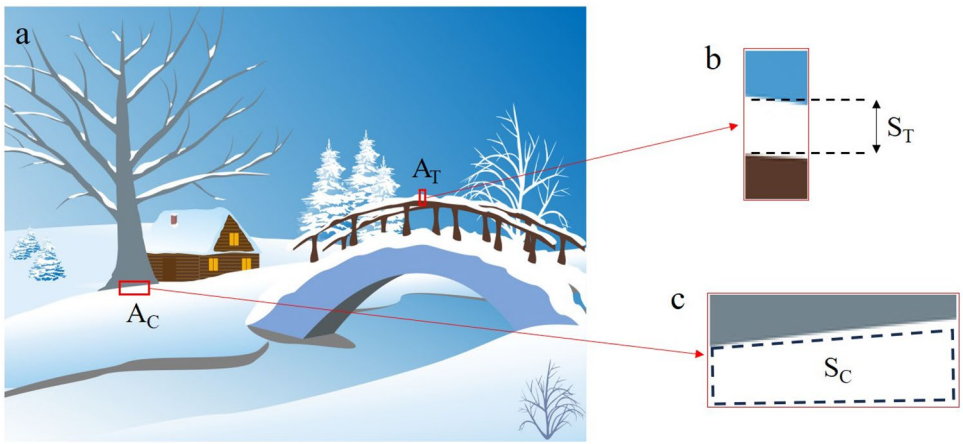


Fig. 2 **a** Example of scene to process; **b**, **c** schematic diagrams for the quantification of the PVI components (parameters: A_C, masked base area of snow; A_T, masked thickness area of snow; S_C, snow coverage; S_T, snow thickness)

the X-axis and red in the Y-axis. Once these quantities are plotted, the algorithm can easily search for the location of the centroid of that group of graphed points. In fact, the position of the centroid allows to identify the type of image in terms of lighting and color. The threshold values and the categorization of the image types to be distinguished must be appropriately calibrated on the basis of the monitored scene and the variability of the predominant environmental conditions.

After distinguishing the different types of images, for each of them, a methodology must be calibrated for recognizing the pixels representing snow and those representing walls or rocks (Fig. 3). This calculation is then automatically performed across all the RGB images collected. Following this method, it is effective to distinguish image tones as well as snow and white-shown rocks on the slope. Once the number of pixels covered by snow is recognized, the percentage of snow coverage can be calculated by dividing the obtained number by the total number of pixels included in A_C.

The second parameter used for identification aims at quantifying the thickness of snow present at the scene. Once S_C is high, in fact, it becomes no longer able to express the accumulation of snow on the ground. For this reason, it is decided to add the second parameter, S_T, which expresses the snow thickness. To attain this,

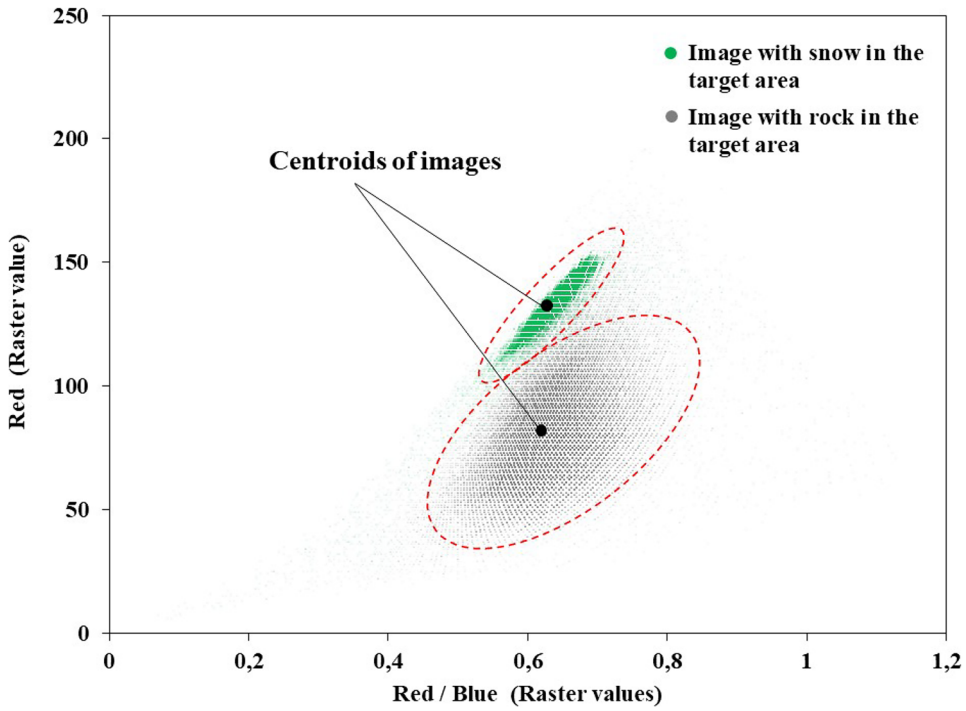


Fig. 3 Separation of snow images from images of white-shown rocks on the base of characteristic RGB patterns

a second area A_T must be masked, identifying a part of the image in which a clear accumulation process is observable, such as house roofs, fence walls, or other objects. In this area, snow thickness is designed to be the ratio of snow pixels to the total masked area and is defined to be a dimensionless value as well as snow coverage. Ultimately, the product of snow coverage (S_C) and snow thickness (S_T) is computed to be a dimensionless variable representing snow as PVI.

Long short-term memory neural network

In this work, long short-term memory (LSTM) neural network is selected to conduct a forecasting mission due to its wide range of uses and ability to handle various types of data. LSTMs are a type of recurrent neural network architecture designed to better capture and remember long-term dependencies in sequential data, especially nonlinear relations among datasets (Fan et al. 2021). In contrast to conventional neural networks, which process input data linearly from start to finish, LSTMs have a recurrent connection that enables them to maintain a hidden state or a memory of past inputs as layer 1 and layer 2 indicate in Fig. 4. This capacity to remember or forget some information makes them particularly adept at tasks involving sequential data or time series (Hochreiter and Schmidhuber 1997). The choice of the number of LSTM layers is determined based on the size of the dataset and the length of the sequences. Increasing the number of layers enhances data processing capacity. Given that this study involves five parameters including temperature, snow, rainfall, humidity, and displacement rate over a time span of 3 years, two LSTM layers are used in testing various configurations. Subsequently, displacement is predicted as the output value.

To gain a precise understanding of the factors influencing landslides, starting from the traditional model coupling only rainfall and displacement (RD model) rate, other combinations of factors are here considered, such as rainfall-snow-displacement (RSD) rate, rainfall-temperature-displacement (RTD) rate, rainfall-humidity-displacement (RHD) rate, rainfall-snow-temperature-displacement (RSTD) rate, and rainfall-snow-temperature-humidity-displacement (RSTHD) rate models. All this is required in order to explore displacement rate trends under different conditions and, finally, select the optimal model.

In order to assess the influence of snowmelt on landslide deformation and the reliability of the early warning model, this paper employs three statistical indicators which are mean squared error (MSE), root mean squared error (RMSE), and mean absolute error (MAE). Among them, MSE weights the square of errors during calculation, making it more sensitive to large errors. This means that in the presence of outliers or anomalies, MSE can be influenced by these values, potentially causing the model to be overly responsive to outliers. MAE treats all errors equally and does not magnify the impact of outliers. RMSE falls between these two as it weights the square of errors but is still influenced by larger errors (Brassington 2017; Karunasingha 2022). Therefore, both RMSE and MAE can offer a more comprehensive perspective, aiming in evaluating the model's performance across various scenarios.

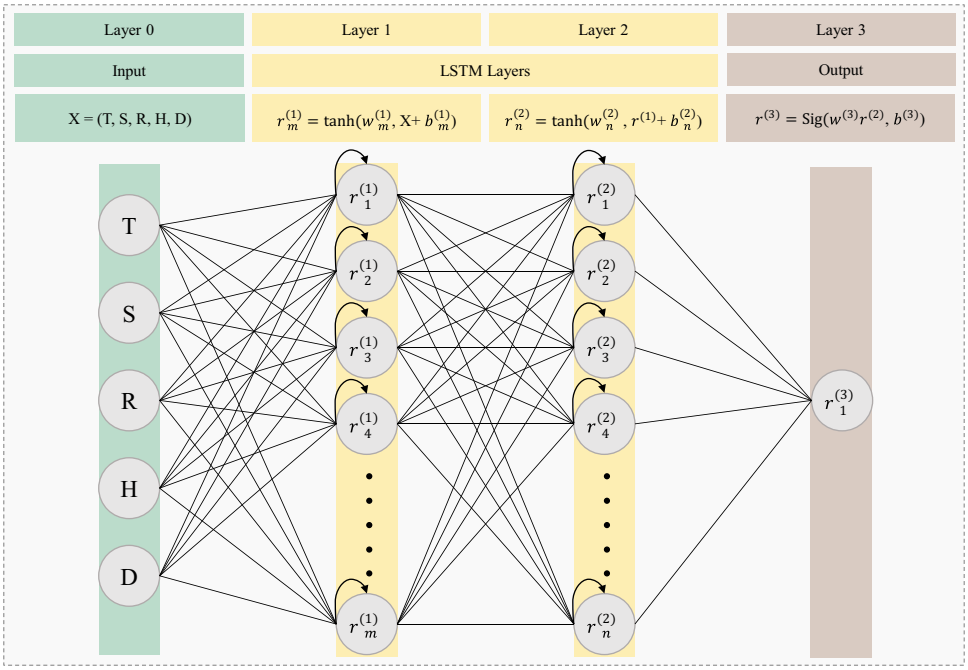


Fig. 4 Structure of the adopted LSTM network: temperature (*T*), snow (*S*), rainfall (*R*), humidity (*H*), and displacement rate (*D*) are the data used as input in layer 0, layer 1, and layer 2 which are LSTM layers and layer 3 is the output layer

Study area

Landslide description

The Sant'Andrea landslide is situated in the Dolomites area of the Northern-Eastern Italian Alps and poses a significant risk to nearby residents (Fig. 5). Its estimated volume is around 60,000 m^3, located in an area of about 72,000 m^2. If the unstable mass collapsed, it could potentially block the Boite river, leading to flooding of the nearby Perarolo di Cadore hamlet and the area downstream (Brezzi et al. 2021a). Extensive geological and geotechnical studies have been conducted to understand the characteristics of the landslide area. The landslide consists of a 30-m-thick layer of clay-calcareous debris, composed of heterogeneous materials with varying grain sizes and geotechnical properties. It slides over weathered bedrock comprised of dolomitic lithology and folded layers rich in anhydrides and gypsum.

The geological and hydrogeological investigations revealed two groundwater flow systems within the landslide area: a shallow system in the upper layers of the debris deposits and a deep system involving the upper part of the bedrock, which contains altered and fractured gypsum. Water plays a crucial role in slope instability, accelerating displacements during intense and prolonged rainfall events and causing slow displacements during dry periods through active water circulation.

The interaction between water and gypsum components of the bedrock and debris layers influences the mechanical properties of the rock mass. Hydration processes result in the plastic rheology of the weak gypsum lithology, as well as the development of karst cavities and microcracks.

Landslide monitoring

Monitoring of Sant'Andrea landslide has been carried out since 2013 using a topographic system with reflective targets installed inside and outside the unstable area. It has provided valuable data on cumulative displacement over time, helping to understand the behavior of the landslide and identify areas of significant displacement. Since 2013, the target configuration has been adapted several times after some episodes in which slope volumes close to the main scarp collapsed, the last of which occurred in June 2021. Figure 6a illustrates the arrangement of monitoring stations before and after this event. A natural collapse occurring in early June produced the detachment of about 8000 m^3 from the front face (Fig. 6b), while on June 25, 2021, a professional team conducted a controlled blasting of about 5000 m^3 on another unstable volume to remove it and mitigate the risk for the downstream area. Following these interventions, based on monitoring data, the landslide appears to gradually reduce its displacement rate, even if not completely stabilized. This is clearly evidenced in Fig. 6, where the displacements developed in a 2-month interval before and after the controlled blasting are superimposed on the target maps.

In addition to the topographic monitoring, in May 2021 a photogrammetric system has been put into official use for monitoring the superficial deformation. The photographic system consists of three Canon EOS 1300D cameras installed on the other side of the Boite valley just at a distance of around 350 m from the Sant'Andrea landslide. Every 15 min, the system prompts the cameras to take pictures and then uploads them to an FTP (File Transfer Protocol) server. On the FTP server, all images can be viewed and downloaded as needed. However, some images captured during the night, heavy fog, or periods of intense rainfall and snowfall, due to their inherent visual disturbances, cannot be effectively utilized. They can only be regarded as references.

Result

Snow quantification algorithms

Snow data is the only data that cannot be directly measured and obtained through a monitoring probe or device. Currently, in fact, there are no related devices installed on the Sant'Andrea landslide that can quantitively monitor snowfall. Therefore, obtaining snow measurements indirectly through the collected images has become the strategy in this research, and the snow recognition algorithms have been developed and applied to it.

To this aim, we purposefully chose a target area according to two criteria. Firstly, we excluded areas densely covered by vegetation or persistently shrouded in shade, as these factors could introduce bias and obscure our findings. Secondly, the area must be correctly oriented with respect to the camera to have an accurate quantification of its cover. Following these criteria, we selected an optimal study area on the right side of the slope as Fig. 7a indicates, which contains 124,206 pixels. Subsequently, the centroid which represents the center of a set of a finite number of selected points (Berele & Catoiu, 2018; Abdi 2009) of each image

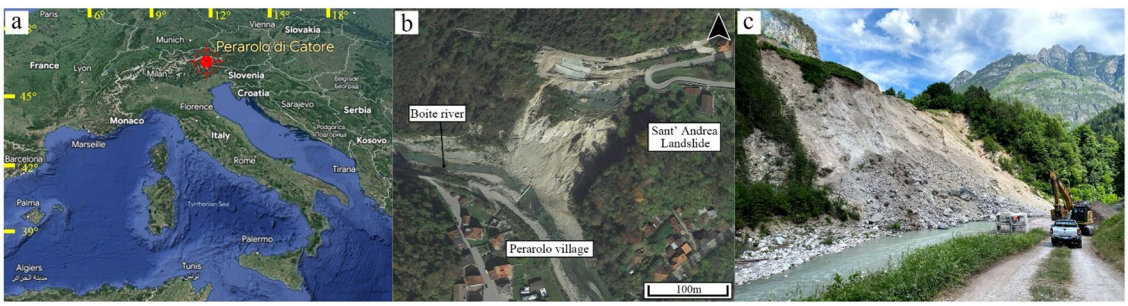


Fig. 5 **a** Location of Sant'Andrea landslide in North-East of Italy (46° 23′ 57″N, 12° 21′ 20″E). **b** Aerial view of Sant'Andrea landslide. **c** Front view of the main scarp

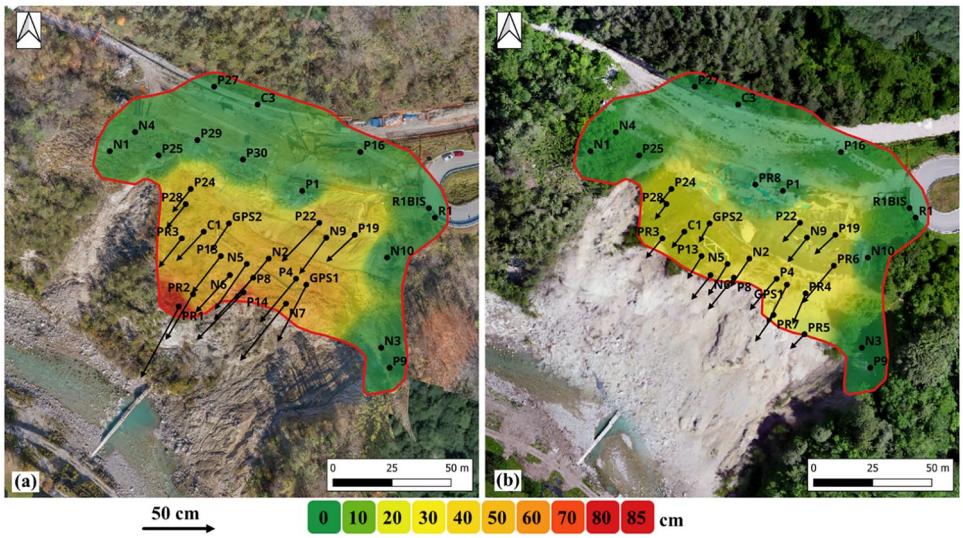


Fig. 6 Positions of topographic targets and colored distribution of the displacement accumulated during the periods **a** April–May 2021 and **b** August–September 2021. The arrows represent the horizontal displacements accumulated at each specific target

is calculated in Fig. 7b. This was necessary because the image tone has a strong interference on recognition and quantification of snow presence. In fact, as later explained, the recognition process is based on the color composition of the selected area, which can vary significantly during the same day (morning, noon, and evening) as well as under different weather conditions (sunny, snowy, and cloudy weather). During different moments in the day and weather conditions, the images can exhibit a mainly bluish, yellowish, reddish, or adequate sunlight, as Fig. 8 shows. Consequently, this variance impacts the RGB values of the object. In general, the brighter the color of an image, the higher the RGB values (Riehle et al. 2020). This leads to RGB values in images captured on sunny days being higher than those taken on cloudy and rainy/snowy weather. Similarly, RGB values for images with a diffuse snow coverage are higher than those without snow coverage. This necessitates the establishment of distinct thresholds for quantifying snow, including snow coverage rate and snow coverage thickness.

Generally, blue-toned images are mostly taken during the early morning and evening at sunrise or sunset, and yellow-toned images are shot during daytime, with cloudy or rainy weather. In addition, weak sunlight can also cause a yellowish tint in the image. Furthermore, it is speculated that during the periods of seasonal transition (spring or fall), some cyclones originating from the south to southwest may carry sand and dust from the Sahara Desert, leading to images with shades of yellow and special brightness tones. On the contrary, when cyclones originate from the north or west, devoid of sand and dust, the color tones change entirely based on the varying intensity of light. Finally, sunlight exposure refers to the condition of direct sunlight on extremely sunny days. Therefore, the image tone differentiation was deciphered using a process based on centroid clustering.

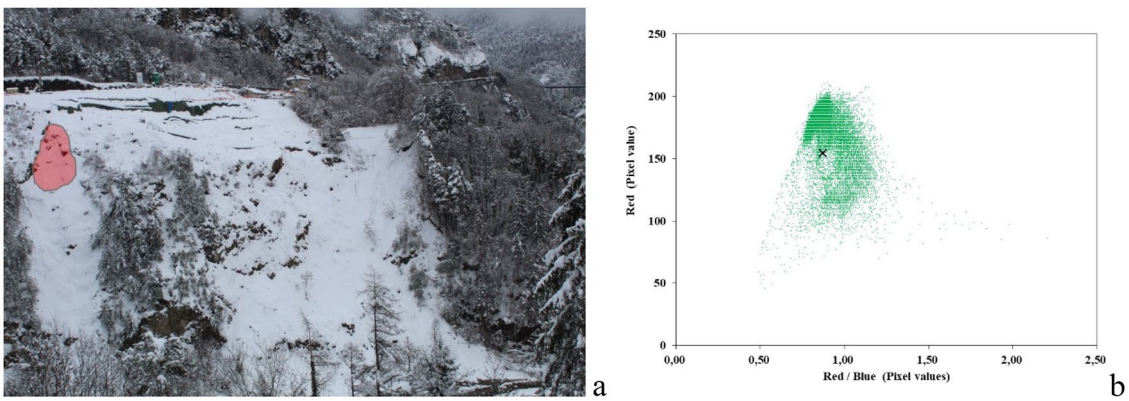


Fig. 7 **a** Selected area for quantifying snow (pink colored area on the left side of the image). **b** Inside the selected area, some points are indicated for the centroid individuation (right coordinate system); "×" represents the centroid of these 124,206 pixels

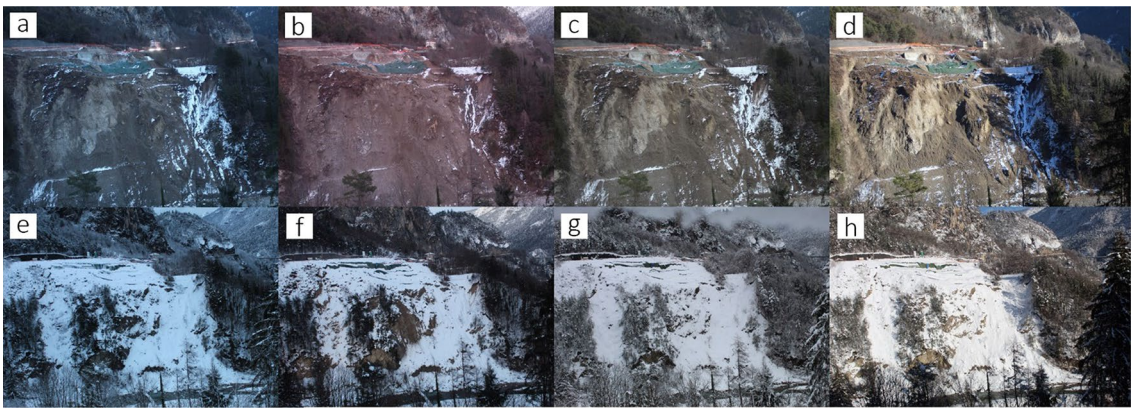


Fig. 8 Image data in four different tones without and with snow on the slope. **a** Bluish image with rock. **b** Yellowish image with rock. **c** Special brightness image with rock. **d** Sunlight image with rock. **e** Bluish image with snow. **f** Yellowish image with snow. **g** Special brightness image with snow. **h** Sunlight image with snow

The masking areas in images with different tones exhibit different centroid distributions. Centroids of the target area in each image are calculated by means of the K-mean clustering method (Likas et al. 2003). The images will be classified into different tones' collection based on the position of the centroid. Figure 9 shows the data related to a test set which includes 50 images, manually selected and categorized to be representative of the four different tones: each point represents the red value vs. red/blue ratio determined by the centroid of the target area in each image. In the same plot, the subdivisions among the four categories are drawn and implemented in an algorithm to divide the entire dataset (4369 images), consisting of 1298 images collected in winter.

The next step in the process of snowfall identification involves identifying the presence of exposed, white rocks on the slope, as shown in Fig. 10b and c. These rocks introduce significant interference in the recognition work. In fact, the algorithm first adopted for snow recognition identified white-shown rocks as snow. To solve this error, the RGB values of all the photos were extracted and analyzed. These data are reported in a plot (Fig. 11) where the X-axis represents the ratio of red value to blue value, while the Y-axis represents the red value. Of course, one R/B vs. R plot for each group of photos needed to be constructed with different color tones. The points appear grouped in two clusters: data referring to the green group represents images showing mostly snow with a few visible rocks, while the gray group comprises conditions where there is no snow at all. The pixel data of the two groups are well separated, making it possible to establish a criterion for effectively distinguishing areas covered by snow from white-shown rocks. The threshold curves were generated accordingly by manually selecting three calibration points and calculating the fitting curve through them (Burton-Johnson and Wyniawskyj 2020). In Fig. 11, the thresholds were manually set

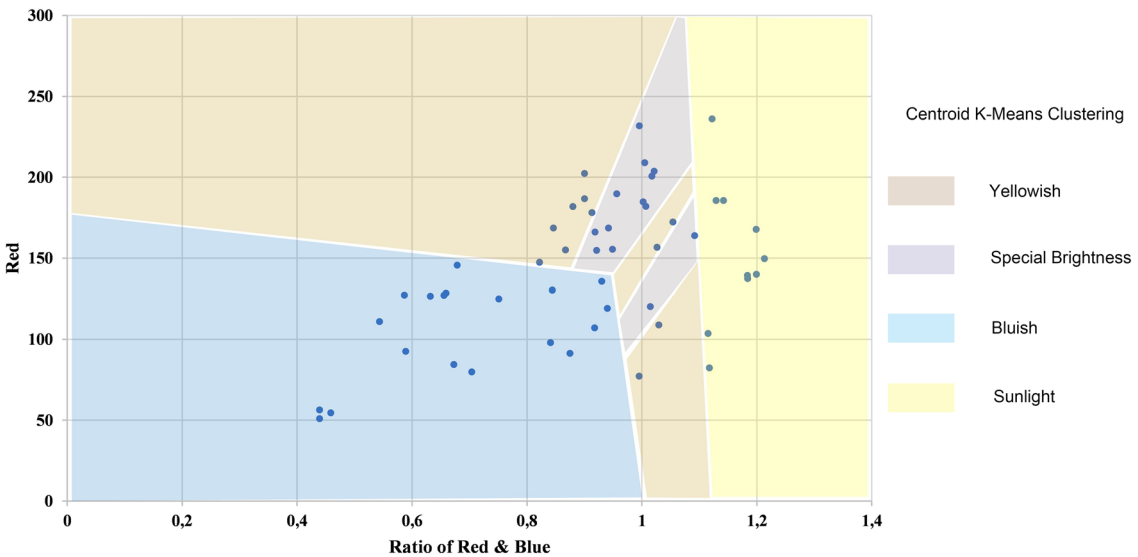


Fig. 9 Range of images' centroid distribution in different tones

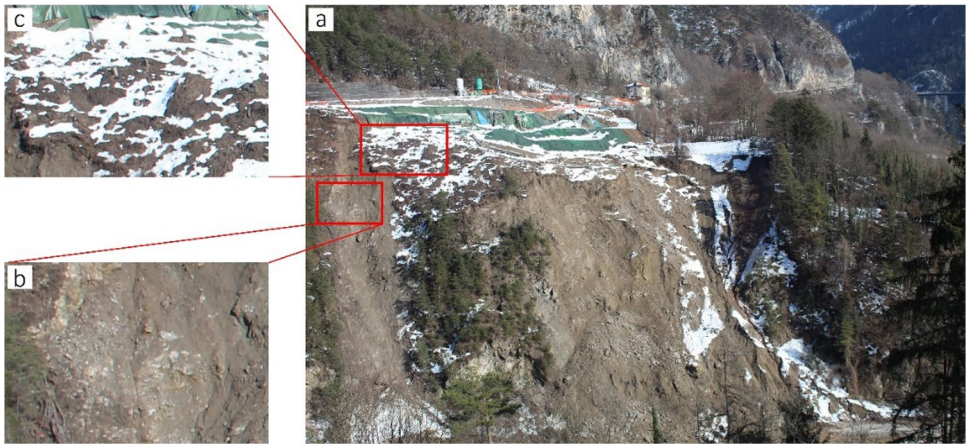


Fig. 10 Separation of snow from exposed white rocks: **a** panorama of landslide with partial snow cover. **b** Exposed white rocks on the slope seen after zooming in. **c** The actual snow seen after zooming in

as either bluish, yellowish, sunlight, or special brightness. Note that the images with relatively complete snow coverage before and after snowfall are predominantly in blue tones: in this case, the distinction between snow and white rocks is quite evident. Additionally, most images acquired during the winter include rocks that are not entirely covered by snow.

Therefore, within the algorithm, different thresholds are set for snowfall detection in different tonal images to ensure the separation between snowfall and white-shown rocks, ultimately identifying the snow coverage in the selected area. We consider the selected area as representative of the whole image, and the recognition results are represented by a coverage percentage.

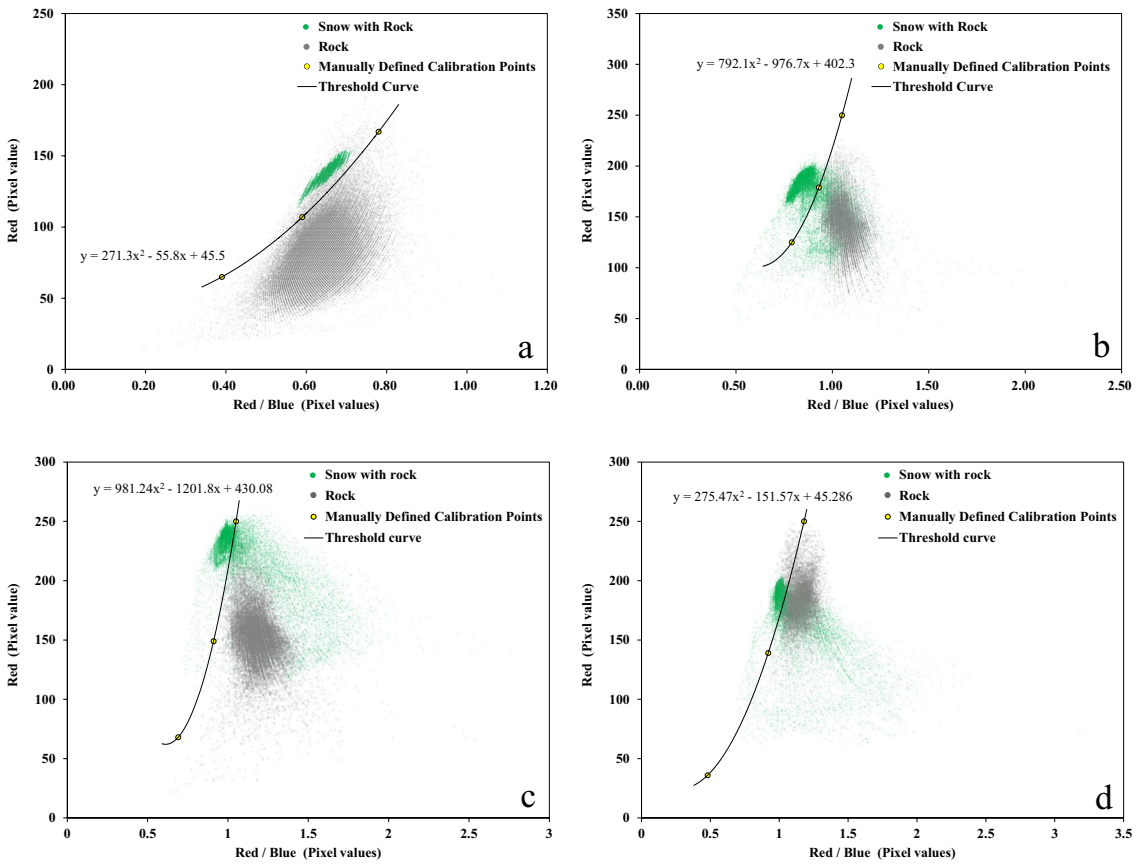


Fig. 11 Separation of snow images from images of white-shown rocks on the basis of characteristic RGB patterns. Thresholds for **a** bluish images, **b** yellowish images, **c** sunlight images, and **d** special brightness images

To quantify the snow presence with accuracy, in addition to coverage percentage, another essential parameter is snow thickness. To achieve this objective, considering the appropriate recognition views and places where it is possible to discern clear boundaries between snow-covered and non-covered areas, the most suitable place to quantify the snow thickness appears to be the top of a retaining wall located at the landslide rear (Fig. 12a). This is because the snow covering the top of this wall is clearly visible and it aligns with the shooting angle, providing a more realistic representation of the snow depth. As Fig. 12 indicates, on the top of the retaining wall (Fig. 12b), a rectangular region of 10 × 40 pixels (Fig. 12c) was selected for snow thickness quantification. Due to the absence of interference from white-shown rocks on the slope, the extracted rectangular area is converted into a binary image (Liu et al. 2012). Then, to identify the boundary between the snow and non-snow zone in the binary image, another criterion is used, for which the boundary localizes a difference of 45 or more in the gray values between the snowy and non-snowy areas. Using this method, as shown in the binary image of Fig. 12c, two distinct boundaries ensue: the upper one represents the boundary between the snow cover and the background behind it, while the lower one represents the boundary between the snow cover and the retaining wall. Finally, after calculating the proportion of snow pixels in each column of the rectangular area, the average proportion of ten columns is used to represent the thickness of the snow, and it is also a dimensionless value as snow coverage. As a result, the thickness of the snow can be identified.

Finally, a new parameter named Pixel Volume Index (PVI) is introduced to visualize the amount of snow. Its definition is:

$$PVI\ [\%] = S_c \cdot S_T \tag{1}$$

where S_C is the snow coverage, representing the percentage of selected area occupied by snow, and S_T is the thickness proportion of snow as explained in Fig. 13. Among all the collected data images, the data with the thickest snow is considered as 100%, and when there is no snow, the thickness is 0%. All other results are expressed as a proportionate percentage of the maximum value after recognition. S_C and S_T are dimensionless indicators as well as PVI whose variation over time can quantify the trends of snow accumulation or melting.

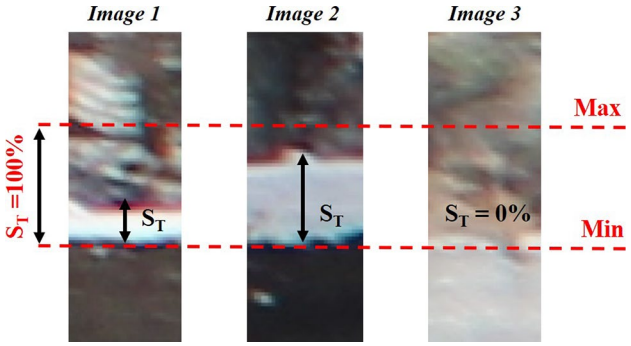


Fig. 13 Illustration of snow thickness under different conditions (Image 1 shows a little snow, image 2 exhibits a large amount of snow, while image 3 indicates no snow)

Snow data visualization

The images captured with the photogrammetric monitoring over 3 years including three winters are collected and used as input dataset. In total, the dataset contains 4369 images.

To quantify the landslide displacement rate, we selected monitoring stations located within the undamaged yellow deformation area in Fig. 6b, i.e., the portion of landslide exhibiting medium displacement rates. Among these, the GPS1 station is considered the most representative since it presents a time series data more regular because it is the less susceptible to effects induced by wind and passage of animals.

The quantitative results of snow PVI, combined with daily rainfall, temperature, humidity, and displacement rate data, are displayed together in Fig. 14, showing their relationship. The snow PVI appropriately captures the changes in snow cover on the Sant'Andrea landslide as highlighted by the dashed boxes. In the northern Italian Alps region, winter 2020–2021 produced heavy snowfalls: two substantial snows occurred on December 28, 2020,

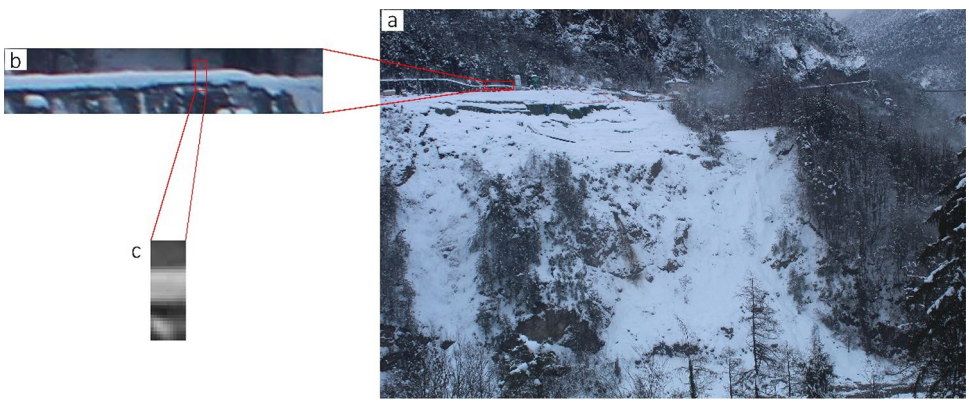


Fig. 12 Extraction of snow thickness in pixel unit from the image: **a** overall image. **b** Detail of the overall image showing the retaining wall at the landslide rear. **c** Selected 10 × 40 pixels area for determination of the snow thickness

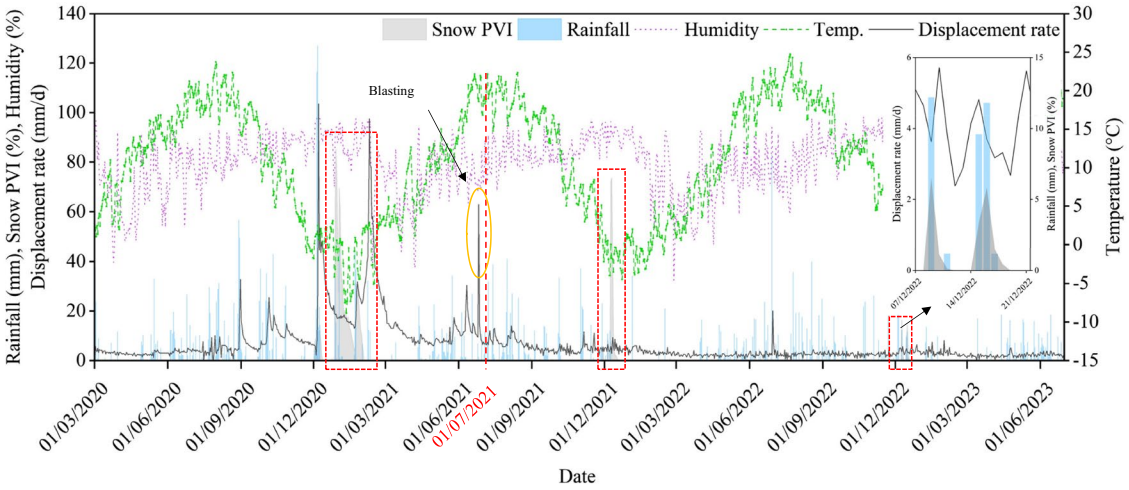


Fig. 14 Snow PVI related to temperature, humidity, and rainfall in the period from March 1, 2020, to June 30, 2023

and on January 2, 2021, during the period of the most intense landslide deformation. In Fig. 14, the snow PVI accurately depicts the accumulation and melting of these two intense snowfalls, while also evidencing the temporal relationship between snowfall, snowmelt, and landslide movement. The snow increased the gravitational load on the landslide and, on the other hand, the melting snow infiltrated on the landslide, thus disrupting the stress balance and causing accelerated deformation. Unfortunately, this effect is not completely determinative because the displacement rate is surely affected also by the large amount of rain that also occurred in the same period. During the winter of 2021–2022, there was only one snowfall, concentrated on December 9, 2021. Its entity was less than the previous year and of shorter duration. Additionally, there were minor rains and a slight acceleration of landslide activity. Finally, the winter of 2022–2023 was particularly warm with temperatures well above the mean values of the area for that period and, as a result, there was virtually no snow.

It is important to note that the landslide exhibits high acceleration not only due to snow. As already demonstrated by Teza et al. (2022), rain is one of the most important factors controlling the mobility of this landslide. But Fig. 14 clearly evidences that also snow has an impact on landslides, which cannot be ignored when analyzing the deformation of the Sant'Andrea landslide.

Displacement forecasting and causal analysis

In order to accurately investigate the influence of snowfall on landslide displacement, various combinations of meteorological parameters are utilized in relation to the displacement rate. Here, R, S, T, H, and D respectively represent daily rainfall, snow PVI, air temperature, air humidity, and surficial displacement rate of the GPS1 monitoring station. Different configurations share the same data segmentation that consists of 373 days (from November 1, 2020, to November 7, 2021) used for training and 266 days (from November 8, 2021, to July 30, 2022) used in the forecasting. The testing of the model is conducted within a range of several combinations, among which some configurations, such as RTD and RHD, consider only temperature and humidity variables associated with rain, and others consider rain in association with snow and temperature (RSTD) or all the factors together (RSTHD). Totally, six combinations are considered.

Figure 15 compares the tests of displacement rates predicted in the forecasting period by the six different configurations. Table 1 lists the values of corresponding reliability indicators. Considering both Fig. 15 and Table 1, it is observed that RSTHD predicted the highest and most unrealistic values for the displacement rate; consequently, it reaches the worst evaluation among all the configurations. RTD and RHD also yield unrealistic results, even if lower than those of RSTHD. In contrast, RD and RSD closely align with the measured displacement rate and exhibit favorable evaluation parameters.

Notably, configurations including snow, such as RSD and RSTD, show an increase in displacement rate following the variation of snow on the slope, the behavior that seemed to occur during winter 2020–2021 and can be theoretically justified. In fact, it is commonly thought that snow melt increases water infiltration and groundwater pressure at the sliding surface, consequently changing the momentum balance of the landslide. The result here obtained successfully demonstrates that snow is one of the factors influencing landslide displacement, but it might be that the weight assigned to snow is too high.

The same consideration can be tested on temperature and humidity: their presence raises the displacement rate too high in the second period. We have attributed the reason for this to the learning pattern of deep learning neural networks. The essence of deep learning neural networks lies in the regression analysis between data, discerning relationships between different data through learning from input data and calculating weights and bias for mutual influences among data points. In this case study, unlike rainfall and snow where values can be zero at times, the values of temperature and humidity are always non-zero and span a wide range. This leads to their consistent presence, and they are therefore assigned a certain weight in the model throughout the learning process when the temperature is very low, thereby elevating the outcome. This also indicates that temperature and humidity, as indirect factors influencing landslide displacement, are not suitable

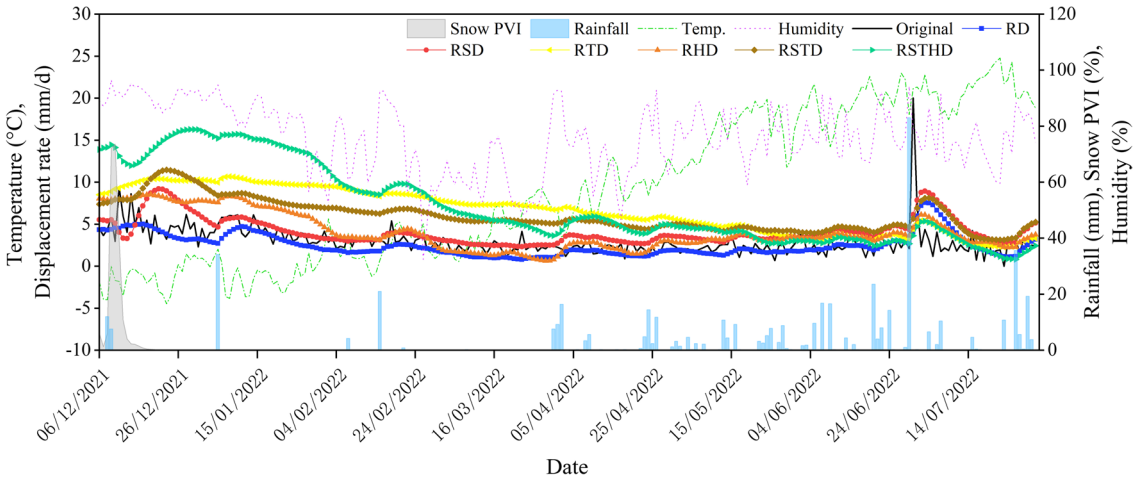


Fig. 15 Comparison of forecasting tests' results of different configurations (original represents the real displacement rate, while *R*, *S*, *T*, *H*, and *D* are rainfall, snow PVI, temperature, humidity, and displacement rate, respectively)

Table 1 Reliability indicators of all the analyzed configurations

Configurations	MAE	MSE	RMSE
RD	1.12	3.01	1.73
RSD	1.48	4.61	2.15
RTD	3.84	19.50	4.42
RHD	1.60	4.83	2.20
RSTD	3.16	12.58	3.55
RSTHD	4.50	34.63	5.89

for being incorporated into the Sant'Andrea displacement forecasting models.

The outcomes suggest that rainfall (RD) is still the most important factor which we should consider firstly; then, the configuration RSD and RSTD curves underwent a delayed displacement change after the snow event. Therefore, the preliminary analysis suggests that snow has an impact on the deformation of the landslide.

Furthermore, when focusing on the two configurations with the best results, RD and RSD, the comparison of the trend of the two curves is unexplainable, since RSD consistently remains higher than RD even after the snow events. However, upon analyzing Figs. 14 and 15, it becomes apparent that after the collapse of June 2021 and the subsequent induced blasting, the landslide motion gradually stabilized toward a quite constant rate. It is natural to think that these events (natural and induced collapses) produced a significant change in the kinematic mechanism of Sant'Andrea landslide, thus resulting in a lack of alignment between RD and RSD predictions along the same level.

Considering the reasons above, the dataset was expanded and the landslide was studied in two phases. Based on the kinematic movement pattern, July 1, 2021, is regarded as a time point that divides the timeline, thereby segmenting the evolution of the landslide into two stages. The first stage spans from March 1, 2020, to June 30, 2021, while the second stage encompasses the period from July 1, 2021, to June 30, 2023. Both stages are utilized to investigate the influencing factors on the landslide and for forecasting purposes, applying only the LSTM model for RD and RSD configurations.

The first stage lasted for 487 days, with 275 days used for the training set and 212 days utilized as the forecasting set. The obtained results are shown in Fig. 16. According to the results, it can be observed that in the first stage, snow variation during winter accelerated the landslide deformation, even if the predictive outcomes do not reach the peak values observed in reality: this indicates that although the model considers both rainfall and snowmelt could predict the landslide acceleration, it could not accurately forecast its displacement magnitude. The predictions based on rainfall are significantly lower than the actual values. Therefore, snow is also an important factor that accelerates landslide deformation in winter.

The reliability indicators of two LSTM models for this stage (Table 2) indicate a relatively poor reliability of both the models, even if the correspondence of predicted values with measured ones according to the trends of Fig. 16 seems effective. This is due to the fact that even if the trend seems well described, especially by the RSD model, there are large differences between the predicted and the original data in correspondence of the peak, which push the reliability indicators toward higher values. In any case, in comparison to the RD configuration, the RSD configuration demonstrated prediction performance that is closer to reality, in particular with regard to the identification of the displacement peak in February 2021. Although the forecasting was slightly delayed and the indicators were not very good, this directly demonstrates that in the first phase, snowmelt played a crucial role in accelerating the displacement rate of the landslide.

As regards the second stage, it spanned 730 days, with 488 days used for the training set and 242 days allocated for the forecasting set. The predicted displacement rates are illustrated in Fig. 17, while

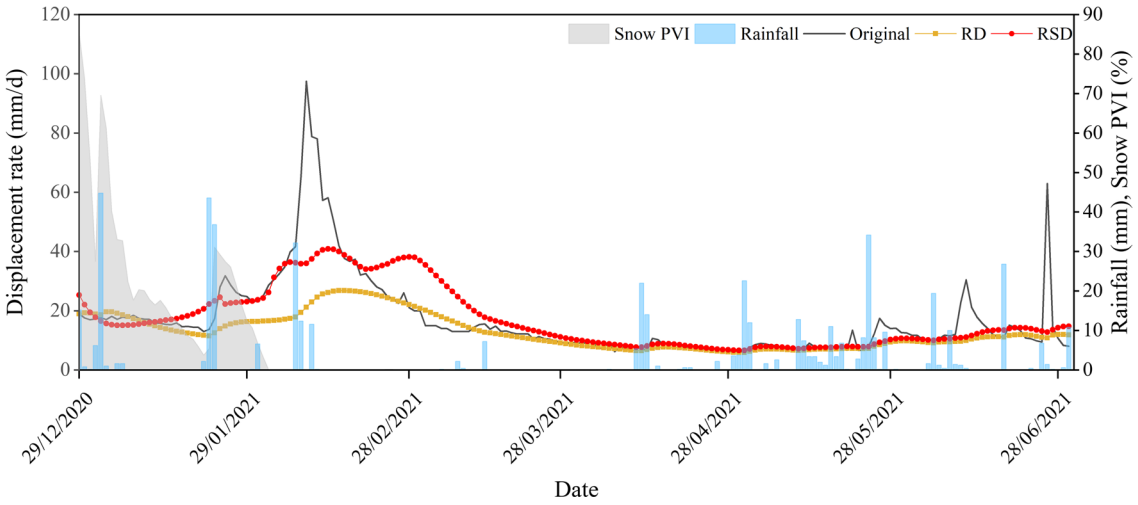


Fig. 16 Forecasting results of 1st period with original displacement rate

Table 2 Reliability indicators of RD and RSD in the 1st stage

Configurations	MAE	MSE	RMSE
RD	5.08	132.52	11.51
RSD	4.67	89.42	9.46

Table 3 summarizes the reliability indicators. On the basis of the outcomes, it can be inferred that in the second stage, the landslide noticeably exhibits smaller deformations and strongly reduced sensitivity to rainfall. Moreover, due to the extremely limited snowfall during the winter of 2023, with only two minor snow events, the snow does not exert a significant impact on the landslide. Nevertheless, the model still proves applicable for predictions in the second stage, with RD and RSD results being quite similar, both satisfying the landslide forecasting requirements. Further exploration depends on future research involving substantial snowfall events that can be utilized.

Table 3 Evaluation parameters of RD and RSD in the 2nd stage

Configurations	MAE	MSE	RMSE
RD	0.68	0.94	0.97
RSD	0.68	0.95	0.97

Table 3 manifests that both RD and RSD exhibited a fundamentally consistent trend and basically identical evaluation parameters, with the differences between each evaluation parameter being less than 0.01. Both can be used for predicting and assessing future trends. However, due to the notably warmer winter from 2022 to 2023, resulting in minimal snowfall, the significance of snowmelt in the deformation of Sant'Andrea landslide during the second stage could not be properly explored. Nonetheless, for future years with

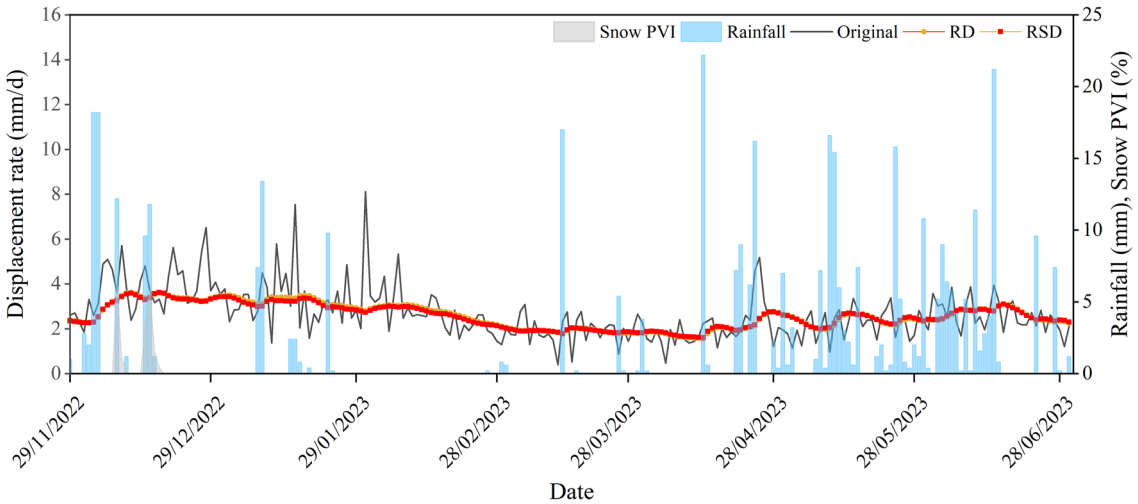


Fig. 17 Forecasting results of 2nd period with original displacement rate

abundant snowfall, model validation and optimization can continue to be applied. Furthermore, similar experiments and exploration can be conducted on landslides situated in higher latitude areas with abundant snowfall.

Finally, to better understand and quantify the impact of snow on landslide movements, a Spearman correlation analysis was conducted to examine the relationship between snow PVI and displacement rate. Figure 18a presents the correlation coefficient for the first period when snow was relatively abundant, while Fig. 18b shows the correlation coefficient for the second period. In the first period, the correlation coefficient is 0.6, indicating a moderate level of correlation between snow PVI and displacement rate (moderate correlation typically ranges from 0.3 to 0.7). In the second period, due to reduced snow in the warmer season, the correlation coefficient decreases to 0.36, but still falls within the moderate correlation range. The significance of the correlation is assessed using a *p*-value, with a *p*-value less than 0.05 indicating that the observed correlation is statistically significant and unlikely to be due to random chance. Overall, these findings suggest a statistically significant, albeit moderate, correlation between snow PVI and displacement rate, underlining the importance of considering snow PVI in forecasting landslide movements.

Discussion

This study combines photogrammetry monitoring and LSTM methods to analyze and predict the displacement rate of landslides. Photogrammetry is specifically used to evaluate the presence of snow on the slope, with the aim of also considering the influence of snow accumulation and melting on the landslide displacement, which is analyzed using LSTM. In previous research, snowfalls have not often been considered comprehensively as rainfalls, and, generally in time series data analysis, rainfall becomes the primary factor in displacement analysis (Brezzi et al. 2021b; Teza et al. 2022, and Nava et al. 2023). However, in high-latitude and high-altitude regions, snowfall occupies a significant duration in winter and is one of the factors that cannot be ignored for landslide study. Additionally, in this study, meteorological factors such as temperature and humidity are considered to complement the analysis of snowfall and snowmelt, providing a valuable exploration of conditions when snow occurs. The paper reveals that the variations of snow can accelerate the displacement rate of landslides to some extent. Also, a moderate positive correlation between the amount of snow and the displacement rate is shown.

From the observation carried out in the first snowy winter, the snow is an important factor affecting the landslide and modifying its stability. Unfortunately, the following winter provided just a few snowfalls, so the relationship between snow and movement does not appear to be so evident. Moreover, the kinematic mode of the Sant'Andrea landslide changed around July 2021 after both the natural and man-induced collapse. The former mode shows large displacement sensitive to rainfall and snow while the latter mode suggests being gradually stable. According to the kinematic movement pattern, July 1, 2021, is treated as a point that divides the timeline, thus splitting the landslide evolution into two stages. The first stage is from March 1, 2020, to June 30, 2021, while the second stage is from July 1, 2021, to June 30, 2023. Both are used to explore the affected factors of landslide and for forecasting. In the first stage, there were significant displacements, and the evaluation parameters for RD deviated notably. Among them, the MAE, MSE, and RMSE reached 5.08, 132.52, and 11.51, respectively. The RSD combination performed even better than RD, with values of 4.67, 89.42, and 9.46. The predictions differed considerably from the actual values at the most intense deformation points, yet simultaneously demonstrated the indispensable role of snow in accelerating landslide displacement. The supposed snow melting process increases the availability of water, which infiltrates the soil and rock layers, thereby raising pore water pressure within the landslide mass. This increase in pore water pressure reduces the effective stress, decreasing the shear strength of the slope materials and making them more prone to movement. The cyclic nature of freezing and thawing also contributes to soil and rock weakening over time, exacerbating deformation. Therefore, it is observed that after the snow thaws, it will gradually infiltrate downwards and exert an influence on landslide deformation. As the infiltration process obviously has a certain lag effect, the maximum snowpack and the maximum landslide deformation are obviously not synchronized. However, in the second stage, there was minimal

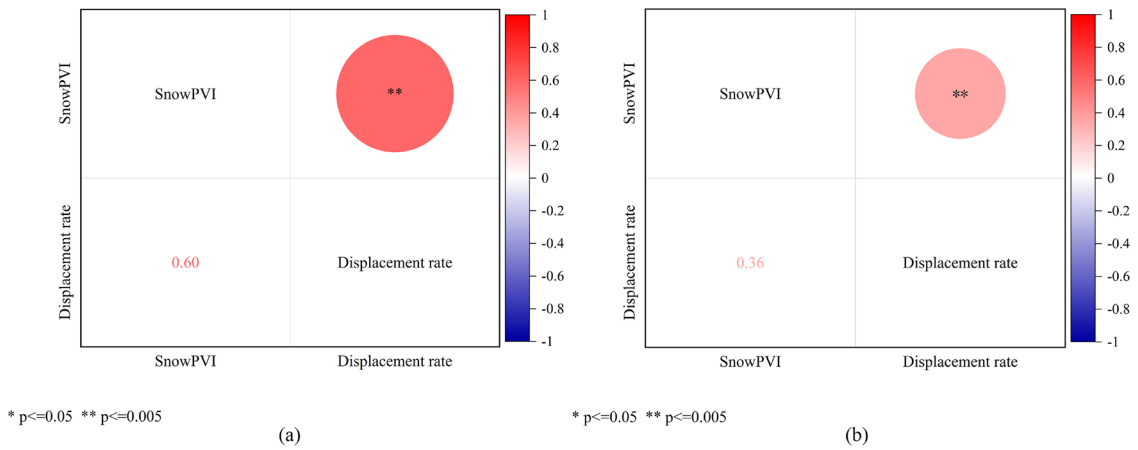


Fig. 18 Spearman correlation analysis between snow PVI and landslide displacement rate (0.6 and 0.36 are correlation coefficients; a smaller *p*-value (**) indicates that the observed correlation is statistically significant)

and stable displacement variation. The predictive evaluation parameters MAE, MSE, and RMSE for both RD and RSD were all less than 1, showing consistent predictive accuracy. In both stages, humidity and temperature decrease the quality of the forecast and do not seem to be significant parameters for this case. As for correlation coefficients of snow PVI and displacement rate within the moderate range, the fact that snow PVI remains at 0 except during winter reversely impacts the correlation level. Therefore, this result supports a significant association between the two variables. Overall, these processes combined make snowmelt a critical factor in the temporal and spatial dynamics of landslide activity, particularly in regions with significant seasonal snow cover.

The basic segment of the model utilizes photogrammetry monitoring, which is a convenient, economical, and direct method. Additionally, with the newly described procedure, the presence of snow has been vividly reconstructed, and its quantification, visualized as a numerical parameter, is introduced into the LSTM network as data from the past 28 days to predict the value for the next day. The LSTM forecast model obtained in this manner demonstrates a relatively straightforward data-driven approach, enabling effective landslide prediction with promising results. However, the suggested method may encounter some difficulties in practical application. For example, in landslides located in remote mountains, problems could arise with monitoring, even when carried out with traditional tools. In our case, for instance, three cameras recording images of the slope were installed from three different positions. Due to inadequate maintenance during the winter, in some periods, we only received monitoring images from one camera. This reduces the possibility for accurate monitoring. Another aspect that complicated the application of LSTM models was the occurrence of natural and man-induced collapses, which significantly altered the kinematic mechanism of the analyzed landslide. This necessitated dividing the monitoring period into two or more stages for separate analysis. The overall dataset had to be subdivided into two parts relative to the periods before and after the collapses in June 2021. Consequently, the data series were reduced and may vary significantly. In the examined case, it was evident that the rainfall-snow configuration yielded the most accurate results in the first period, while both rainfall and rainfall-snow configurations performed well in the second period, particularly as snowfall reduced in intensity and frequency. From an operational perspective, one possible drawback is that the pixel volume index is a value that can reflect the process of snowfall and melting, but when the snowfall is very intense, even if it is possible to capture images from three cameras, the reference points for quantification of snow thickness are covered by snow. This poses a significant challenge to the reconstruction of the real snow accumulation process.

Due to the reasons above, the proposed method would be useful and convenient in specific circumstances. For instance, the snowfall amount should not be too low. Since the melting and infiltration of snow take longer than rainfall of equivalent intensity, snow is generally not considered a triggering factor for landslides. In winter 2022, for example, the warm weather rendered the effect of snowfall negligible. Additionally, this method is best applied to natural landslides that have not been disturbed by human activities, as human interventions may affect the accuracy of prediction models. Finally, for the collection of image data, the landslide location should be relatively accessible to facilitate maintenance. Apart from the mentioned limitations, this method offers a cost-effective and convenient approach for landslide monitoring and early warning.

Ultimately, it is important to emphasize that, in future research, it would be necessary to incorporate groundwater table data into this prediction model to investigate the thermo-hydraulic coupling process of landslide deformation. Unfortunately, in this case, no hydraulic data were available to delve into the physical mechanism of the snow melting phenomenon.

Conclusion

The method proposed in this paper offers a new approach for addressing landslides in snow-covered regions. To summarize the role of snow in the Sant'Andrea landslide, in the first stage, both rainfall and snowfall impact the landslide displacement rate, albeit with a delay, as it takes time for the rainfall and snowmelt to infiltrate into the soil. Rainfall consistently emerges as the most significant and frequent factor affecting the Sant'Andrea landslide year by year. However, during winter, snowmelt also plays an indispensable role in influencing deformation. Furthermore, a moderate positive correlation exists between snow amount and landslide displacement rate. This highlights a mixed level of significance of snowmelt in the Alpine region of northern Italy.

Moreover, the integration of two techniques enables the incorporation of snow into the prediction model. Using photogrammetric measurement techniques to monitor the Sant'Andrea landslide is advantageous due to its economic, convenient, and real-time transmission characteristics. Additionally, in the absence of dedicated snow monitoring devices on the slope, the image-based snow quantification procedure can be applied to reconstruct the snowfall and melting processes, thereby providing a more comprehensive explanation for landslide deformation.

Regardless, 3 years constitute a relatively short observational period, which is insufficient for drawing definitive conclusions. Despite the scarcity of snow limiting its intensive application in LSTM modeling, the preliminary results presented here are promising for the proposed method of incorporating snow influence. This method is innovative and straightforward, with potential applications in future observations during subsequent winters in Perarolo di Cadore or in other possible sites.

Funding

Open access funding provided by Università degli Studi di Padova within the CRUI-CARE Agreement. The research was financially supported by the Fondazione Cariverona through the research grant titled "Monitoring of Natural Hazards and Protective Structures Using Computer Vision Techniques for Environmental Safety and Preservation" and by the Veneto Region through the grant "Scientific Support for the Characterization of Hydrogeological Risk and the Evaluation of the Effectiveness of Interventions Related to the Landslide Phenomenon of Busa del Cristo in Perarolo di Cadore (BL) through the Development of Predictive Geo-Hydrological Models".

Data Availability

The meteorological data presented in this study can be freely downloaded from https://www.ambienteveneto.it. Other data will be made available on reasonable request.

Declarations

Competing interest The authors declare that they have no known competing financial interests or personal relationships that could have appeared to influence the work reported in this paper.

Open Access This article is licensed under a Creative Commons Attribution 4.0 International License, which permits use, sharing, adaptation, distribution and reproduction in any medium or format, as long as you give appropriate credit to the original author(s) and the source, provide a link to the Creative Commons licence, and indicate if changes were made. The images or other third party material in this article are included in the article's Creative Commons licence, unless indicated otherwise in a credit line to the material. If material is not included in the article's Creative Commons licence and your intended use is not permitted by statutory regulation or exceeds the permitted use, you will need to obtain permission directly from the copyright holder. To view a copy of this licence, visit http://creativecommons.org/licenses/by/4.0/.

References

Berele A, Catoiu S (2018) Bisecting the perimeter of a triangle. Math Mag 91(2):121–133. https://doi.org/10.1080/0025570X.2017.1418589

Abdi H (2009) Centroids. Wiley Interdisciplinary Reviews: Computational Statistics 1(2):259–260. https://doi.org/10.1002/wics.31

Bajni G, Camera CAS, Apuani T (2021) Deciphering meteorological influencing factors for Alpine rockfalls: a case study in Aosta Valley. Landslides 18:3279–3298. https://doi.org/10.1007/s10346-021-01697-3

Bishop CM (1995) 1995. Oxford University Press, New York, Neural networks for pattern recognition

Brassington G (2017) Mean absolute error and root mean square error: which is the better metric for assessing model performance? In EGU General Assembly Conference Abstracts, p 3574

Brezzi L, Carraro E, Pasa D, Teza G, Cola S, Galgaro A (2021a) Post-Collapse Evolution of a Rapid Landslide from Sequential Analysis with FE and SPH-Based Models. Geosciences 11(9):364. https://doi.org/10.3390/geosciences11090364

Brezzi L, Gabrieli F, Cola S, Lorenzetti G, Spiezia N, Bisson A, Allegrini M (2020) Digital terrestrial stereo-photogrammetry for monitoring landslide displacements: a case study in Recoaro Terme (VI). Geotechnical Research for Land Protection and Development. CNRIG 2019. Lecture Notes in Civil Engineering 40:155–163. https://doi.org/10.1007/978-3-030-21359-6_17

Brezzi L, Vallisari D, Carraro E, Teza G, Pol A, Liang Z, Gabrieli F, Cola S, Galgaro A (2021b) Digital terrestrial photogrammetry for a dense monitoring of the surficial displacements of a landslide. Eurock (2021b) IOP Conference Series: Earth and Environmental Science, Volume 833. Mechanics and Rock Engineering, from Theory to Practice, Turin, Italy. https://doi.org/10.1088/1755-1315/833/1/012145

Burton-Johnson A, Wyniawskyj NS (2020) Rock and snow differentiation from colour (RGB) images. The Cryosphere Discuss [preprint]. https://doi.org/10.5194/tc-2020-115

Chiarelli DD, Galizzi M, Bocchiola D, Rosso R, Rulli MC (2023) Modeling snowmelt influence on shallow landslides in Tartano valley. Italian Alps Sci Total Environ 856:158772. https://doi.org/10.1016/j.scitotenv.2022.158772

Durand Y, Laternser M, Giraud G, Etchevers P, Lesaffre B, Mérindol L (2009) Reanalysis of climate in the French Alps (1958–2002). J Appl Meteorol Clim 48:429–449. https://doi.org/10.1175/2008JAMC1808.1

Fan D, Sun H, Yao J, Zhang K, Yan X, Sun Z (2021) Well production forecasting based on ARIMA-LSTM model considering manual operations. Energy 220:119708. https://doi.org/10.1016/j.energy.2020.119708

Feizizadeh B, Garajeh MK, Lakes T, Blaschke T (2021) A deep learning convolutional neural network algorithm for detecting saline flow sources and mapping the environmental impacts of the Urmia Lake drought in Iran. CATENA 207:105585. https://doi.org/10.1016/j.catena.2021.105585

Gabrieli F, Corain L, Vettore L (2016) A low-cost landslide displacement activity assessment from time-lapse photogrammetry and rainfall data: application to the Tessina landslide site. Geomorphology 269:56–74. https://doi.org/10.1016/j.geomorph.2016.06.030

Graves A (2012) Long short-term memory. In: Supervised sequence labelling with recurrent neural networks. Studies in Computational Intelligence, vol 385. Springer, Berlin, Heidelberg. https://doi.org/10.1007/978-3-642-24797-2_4

Guzzetti F (2000) Landslide fatalities and the evaluation of landslide risk in Italy. Eng Geol 58:89–107. https://doi.org/10.1016/S0013-7952(00)00047-8

Has B, Noro T, Maruyama K, Nakamura A, Ogawa K, Onoda S (2012) Characteristics of earthquake-induced landslides in a heavy snowfall region—landslides triggered by the northern Nagano prefecture earthquake, March 12, 2011, Japan. Landslides 9:539–546. https://doi.org/10.1007/s10346-012-0344-6

Harris C, Arenson LU, Christiansen HH, Etzelmuller B, Frauenfelder R, Gruber S, Haeberli W, Vonder Muhll D (2009) Permafrost and climate in Europe: monitoring and modelling thermal, geomorphological and geotechnical responses. Earth Sci Rev 92(3–4):117–171. https://doi.org/10.1016/j.earscirev.2008.12.002

Hinds ES, Lu N, Mirus BB, Godt JW, Wayllace A (2021) Evaluation of techniques for mitigating snowmelt infiltration-induced landsliding in a highway embankment. Eng Geol 291:106240. https://doi.org/10.1016/j.enggeo.2021.106240

Hochreiter S, Schmidhuber J (1997) Long short-term memory. Neural Comput 9(8):1735–1780. https://doi.org/10.1162/neco.1997.9.8.1735

Jakob M, Holm K, Lange O, Schwab JW (2006) Hydrometeorological thresholds for landslide initiation and forest operation shutdowns on the north coast of British Columbia. Landslides 3:228–238. https://doi.org/10.1007/s10346-006-0044-1

Karunasingha DSK (2022) Root mean square error or mean absolute error? Use their ratio as well. Inf Sci 585:609–629. https://doi.org/10.1016/j.ins.2021.11.036

Kirschbaum DB, Adler R, Hong Y, Hill S, Lerner-Lam A (2009) A global landslide catalog for hazard applications: method, results, and limitations. Nat Hazards 52:561–575. https://doi.org/10.1007/s11069-009-9401-4

Laribi A, Walstra J, Ougrine M, Seridi A, Dechemi N (2015) Use of digital photogrammetry for the study of unstable slopes in urban areas: case study of the El Biar landslide, Algiers. Eng Geol 187:73–83. https://doi.org/10.1016/j.enggeo.2014.12.018

LeCun Y, Bengio Y, Hinton G (2015) Deep learning. Nature 521:436–444. https://doi.org/10.1038/nature14539

Likas A, Vlassis N, Verbeek J (2003) The global k-means clustering algorithm. Pattern Recogn 36:451–461. https://doi.org/10.1016/S0031-3203(02)00060-2

Liu L, Zhang Q, Wei X (2012) A RGB image encryption algorithm based on DNA encoding and chaos map. Comput Electr Eng 38:1240–1248. https://doi.org/10.1016/j.compeleceng.2012.02.007

Liu YT, Teza G, Nava L, Chang ZL, Shang M, Xiong DB, Cola S (2024) Deformation evaluation and displacement forecasting of baishuihe landslide after stabilization based on continuous wavelet transform and deep learning. Nat Hazards. https://doi.org/10.1007/s11069-024-06580-7

Martelloni G, Segoni S, Lagomarsino D, Fanti R, Catani F (2012) Snow accumulation-melting model (SAMM) for integrated use in regional scale landslide early warning systems. Hydrol Earth Syst Sci Discuss 9:9391–9423. https://doi.org/10.5194/hess-17-1229-2013

Matsuura S, Asano S, Okamoto T, Takeuchi Y (2003) Characteristics of the displacement of a landslide with shallow sliding surface in a heavy

snow district of Japan. Eng Geol 69(1–2):15–35. https://doi.org/10.1016/S0013-7952(02)00245-4
Medsker L, Jain LC (1999) Recurrent neural networks: design and applications. CRC Press
Mondini AC, Guzzetti F, Melillo M (2023) Deep learning forecast of rainfall-induced shallow landslides. Nat Commun 14:2466. https://doi.org/10.1038/s41467-023-38135-y
Ngo PTT, Panahi M, Khosravi K, Ghorbanzadeh O, Kariminejad N, Cerda A, Lee S (2021) Evaluation of deep learning algorithms for national scale landslide susceptibility mapping of Iran. Geosci Front 12(2):505–519. https://doi.org/10.1016/j.gsf.2020.06.013
Nava L, Carraro E, Reyes-Carmona C, Puliero S, Bhuyan K, Rosi A, Monserrat O, Floris M, Meena SR, Galve JP, Catani F (2023) Landslide displacement forecasting using deep learning and monitoring data across selected sites. Landslides. https://doi.org/10.1007/s10346-023-02104-9
Okamoto T, Matsuura S, Larsen JO, Asano S, Abe K (2018) The response of pore water pressure to snow accumulation on a low-permeability clay landslide. Eng Geol 242:130–141. https://doi.org/10.1016/j.enggeo.2018.06.002
Osawa H, Matsuura S, Matsushi Y, Okamoto T (2017) Seasonal change in permeability of surface soils on a slow-moving landslide in a heavy snow region. Eng Geol 221:1–9. https://doi.org/10.1016/j.enggeo.2017.02.019
Osawa H, Matsushi Y, Matsuura S, Okamoto T (2024) Semiempirical modeling of the transient response of pore pressure to rainfall and snowmelt in a dormant landslide. Landslides 21:245–256. https://doi.org/10.1007/s10346-023-02158-9
Pan B (2018) Digital image correlation for surface deformation measurement: historical developments, recent advances and future goals. Meas Sci Technol 29:082001. https://doi.org/10.1088/1361-6501/aac55b
Panzeri L, Mondani M, Taddia G, Papini M, Longoni L (2022) Analysis of snowmelt as a triggering factor for shallow landslide. International Multidisciplinary Scientific GeoConference: SGEM 22(1.1):77–83. https://doi.org/10.5593/sgem2022/1.1/s02.009
Prakash N, Manconi A, Loew S (2020) Mapping landslides on EO data: performance of deep learning models vs. traditional machine learning models. Remote Sens 12(3):346. https://doi.org/10.3390/rs12030346
Riehle D, Reiser D, Griepentrog HW (2020) Robust index-based semantic plant/background segmentation for RGB- images. Comput Electron Agric 169:105201. https://doi.org/10.1016/j.compag.2019.105201
Sameen MI, Pradhan B, Lee S (2020) Application of convolutional neural networks featuring Bayesian optimization for landslide susceptibility assessment. CATENA 186:104249. https://doi.org/10.1016/j.catena.2019.104249
Saez JL, Corona C, Stoffel M, Berger F (2013) Climate change increases frequency of shallow spring landslides in the French Alps. Geology 41(5):619–622. https://doi.org/10.1130/G34098.1
Sassa K, Fukuoka H, Wang FW, Wang GH (2005) Dynamic properties of earthquake-induced large-scale rapid landslides within past landslide masses. Landslides 2:125–134. https://doi.org/10.1007/s10346-005-0055-3
Son H, Lee J, Lee J, Cho S, Lee S (2021) Recurrent video deblurring with blur-invariant motion estimation and pixel volumes. ACM Transactions on Graphics (TOG) 40(5):1–18. https://doi.org/10.1145/3453720
Stumpf A, Malet JP, Allemand P, Pierrot-Deseilligny M, Skupinski G (2015) Ground-based multi-view photogrammetry for the monitoring of landslide deformation and erosion. Geomorphology 231:130–145. https://doi.org/10.1016/j.geomorph.2014.10.039
Subramanian SS, Fan X, Yunus AP, Van Asch T, Scaringi G, Xu Q, Dai L, Ishikawa T, Huang R (2020) A sequentially coupled catchment-scale numerical model for snowmelt-induced soil slope instabilities. J Geophys Res Earth Surf 125(5):e2019JF005468. https://doi.org/10.1029/2019JF005468
Subramanian SS, Ishikawa T, Tokoro T (2017) Stability assessment approach for soil slopes in seasonal cold regions. Eng Geol 221:154–169. https://doi.org/10.1016/j.enggeo.2017.03.008
Teza G, Cola S, Brezzi L, Galgaro A (2022) Wadenow: a Matlab toolbox for early forecasting of the velocity trend of a rainfall-triggered landslide by means of continuous wavelet transform and deep learning. Geosciences 12(5):205. https://doi.org/10.3390/geosciences12050205
Van Houdt G, Mosquera C, Nápoles G (2020) A review on the long short-term memory model. Artif Intell Rev 53:5929–5955. https://doi.org/10.1007/s10462-020-09838-1
Xian Y, Wei XL, Zhou HB, Chen N, Liu Y, Liu F, Sun H (2022) Snowmelt-triggered reactivation of a loess landslide in Yili, Xinjiang, China: mode and mechanism. Landslides 19(8):1843–1860. https://doi.org/10.1007/s10346-022-01879-7
Xu S, Niu R (2018) Displacement prediction of Baijiabao landslide based on empirical mode decomposition and long short-term memory neural network in Three Gorges area, China. Comput Geosci 111:87–96. https://doi.org/10.1016/j.cageo.2017.10.013
Yang B, Yin K, Lacasse S, Liu Z (2019) Time series analysis and long short-term memory neural network to predict landslide displacement. Landslides 16:677–694. https://doi.org/10.1007/s10346-018-01127-x
Ye X, Zhu HH, Chang FN, Xie TC, Tian F, Zhang W, Catani F (2024a) Revisiting spatiotemporal evolution process and mechanism of a giant reservoir landslide during weather extremes. Eng Geol 332:107480. https://doi.org/10.1016/j.enggeo.2024.107480
Ye X, Zhu HH, Wang J, Zheng WJ, Zhang W, Schenato L, Pasuto A, Catani F (2024b) Towards hydrometeorological thresholds of reservoir-induced landslide from subsurface strain observations. Sci China Technol Sci. https://doi.org/10.1007/s11431-023-2657-3
Yin YP, Wang FW, Sun P (2009) Landslide hazards triggered by the 2008 Wenchuan earthquake, Sichuan, China. Landslides 6:139–152. https://doi.org/10.1007/s10346-009-0148-5
Zou ZX, Luo T, Zhang S, Duan HJ, Li SW, Deng YD, Wang J (2023) A novel method to evaluate the time-dependent stability of reservoir landslides: exemplified by Outang landslide in the Three Gorges Reservoir. Landslides 20:1731–1746. https://doi.org/10.1007/s10346-023-02056-0

Yuting Liu · Lorenzo Brezzi (✉) · Fabio Gabrieli · Simonetta Cola
Department of Civil, Environmental and Architectural Engineering, University of Padua, Via Ognissanti, 39, 35131 Padua, Italy
Email: lorenzo.brezzi@unipd.it

Zhipeng Liang
School of Resources and Safety Engineering, Central South University, Changsha 410083, China

Zihan Zhou
Department of Civil Engineering, Tsinghua University, Beijing 100084, China